THE ASTROPHYSICAL JOURNAL, 567:610–621, 2002 March 1

MICROWAVE DETECTION OF SHOCK AND ASSOCIATED ELECTRON BEAM FORMATION

H. AURASS
Astrophysikalisches Institut Potsdam, An der Sternwarte 16, D-14482 Potsdam, Germany; haurass@aip.de
K. SHIBASAKI
Nobeyama Radio Observatory, National Astronomical Observatory, Minamimaki, Minamisaku, Nagano 384-1305, Japan
M. REINER
Raytheon STX, 4400 Forbes Boulevard, Lanham, MD 20706; and NASA Goddard Space Flight Center, Code 690.2, Greenbelt, MD 20771
AND
M. KARLICKÝ
Astronomical Observatory Ondřejov, Czech Republic
Received 2001 April 10; accepted 2001 November 1

ABSTRACT

We use complementary European and Japanese solar radio ground-based observations, together with *Yohkoh* soft X-ray and *SOHO* extreme-UV images, to search for the signature of flare-related waves at different heights above the Sun. The key data set for event selection is 40–800 MHz dynamic radio spectra from the Potsdam Astrophysical Institute, whose radio spectral polarimeter is sensitive to the coronal shock waves due to the associated type II radio bursts in the range between 0.2 and 1 $R_\odot$. Nobeyama Radio Heliograph images at 17 GHz show the chromosphere and the transition region to the corona with unprecedented sensitivity and time resolution (1 s image cadence). Here we focused on 17 GHz images in the time interval between flare onset and the start of the metric type II burst. The decametric–hectometric (Dm–Hm; 1–14 MHz) radio experiment on board *Wind* completes the radio spectral coverage. The spectra are used to check if the coronal shock wave is also continuously visible in the range 3–8 $R_\odot$ and if the corona is open or closed for electron beams exciting hectometric type III bursts. We selected two flare events that show metric type II bursts, but with different associated 17 GHz features. For both events we find flare disturbances in 17 GHz images that propagate earlier than the type II bursts: a hot, dense blob (event 1; 1997 April 2) or a cold, absorbing cloud (event 2; 1998 July 31). In event 1, the hot and dense blob preceded the formation of a wave front segment that appeared in *SOHO*/EIT images. In event 2, we observed the impact of the 17 GHz absorbing cloud on a preexisting quiescent prominence far out of the flaring active region after several minutes of propagation without being disturbed. We demonstrate that the spectral pattern, as well as the drift rate, of the given type II burst drastically changes shortly before the cloud's impact. The Dm–Hm spectra in event 2 reveal a typical shock-associated (SA) event in the outer corona during the interaction between the absorbing cloud and the prominence. Finally, we stress that there may be a common driver for the metric type II bursts and simultaneous decimeter reverse-drift bursts between 1 and 2 GHz recorded on the radio spectrograph of Astronomical Observatory Ondřejov.

Subject headings: shock waves — Sun: flares — Sun: radio radiation

1. INTRODUCTION

Coronal and interplanetary shock waves are a transient source of nonthermal electrons, as revealed by their type II burst radio signature (see Nelson & Melrose 1985 for radio and type II burst terminology). Radio spectra, including coronal type II bursts, are observed at the Potsdam Astrophysical Institute (AI Potsdam) in the range between 40 and 800 MHz (Mann et al. 1992). Digitally processed type II burst spectra and renewed discussion about the driver of coronal/interplanetary shock waves (see, e.g., Mann, Classen, & Aurass 1995; Cliver, Webb, & Howard 1999) stimulated an improvement of our knowledge about shock waves in the coronal plasma. The type II burst spectrum consists of slowly drifting lanes (the backbone) at the fundamental and higher modes of the plasma frequency. Superposed are specific narrowband fast-drift bursts, called herringbones (Nelson & Melrose 1985). Some herringbone bursts escape from the backbone with positive frequency drift (exciter moves toward rising density), others with negative drift (exciter moves toward decaying density). This suggests electron acceleration at the coronal shock fronts (see Mann 1995 for a review). Klassen et al. (1999) discovered radio precursors of the shock-exciting disturbance that fills in the "time and frequency gap" in the dynamic spectrum between the impulsive flare phase and the start of the metric type II burst at frequencies below 150 MHz (fundamental mode). Spatially, these faint radio sources occur between the chromospheric flare and the radio type II burst site. Vršnak & Lulič (2000a, 2000b) explained the physical significance of the type II burst precursors. Klein et al. (1999) presented a case where a soft X-ray signature in a loop ensemble precedes a metric type II burst source. Hudson & Karlický (2000) have shown for the first time a high-frequency (1–2 GHz) precursor of type II emission, together with a wave indication in *Yohkoh* soft X-ray images.

Using the Extreme-Ultraviolet Imaging Telescope (EIT) on board the *Solar and Heliospheric Observatory* (*SOHO*), there was discovered a new flare-related coronal wave phenomenon (Thompson et al. 1998) that is well associated with coronal shocks (type II bursts) in time but seems to

propagate with only about one-third of the speed inferred from the type II bursts (Klassen et al. 2000). The relationship among the type II bursts, EIT waves, and the chromospheric Moreton waves seen in Hα images (see, e.g., Moreton & Ramsey 1960) is described in some case studies (Warmuth et al. 2000; Pohjolainen et al. 2001; Thompson et al. 2000). Warmuth et al. (2001) stress that the speed discrepancy among Moreton waves, type II bursts, and EIT waves may be due to an observational bias. For one event, Khan & Aurass (2001) identify a moving soft X-ray disturbance, the corresponding metric type II radio source sites, an EIT wave, and a Moreton wave caused by the same flare energy release.

The existence of type II radio bursts is the main evidence for the acceleration of electrons at coronal shock waves. Sometimes, type II bursts are associated with bunches of fast-drift bursts (type III bursts) that can be observed up to the Hm wavelength range. The type III burst spectrum emanates from the type II burst lanes. Therefore, Cane et al. (1981) introduced the term "shock-accelerated" (SA) events. SA can also be interpreted as "shock-associated," if there is no spatial coincidence of the type III and the type II radio sources.

Type III bursts are the most frequently occurring fast-drift bursts (see, e.g., Suzuki & Dulk 1985). The type III sources trace the magnetic connectivity of field lines rooted near the electron beam acceleration site. Klein et al. (1997) demonstrate that a destabilized prominence-supporting streamer configuration reacts by spurious electron beam injections, leading to fast-drift bursts from coronal electron injection heights of about 1 $R_\odot$ above the photosphere. We use low-frequency radio spectra (1–14 MHz) observed by the WAVES instrument on *Wind* (Bougeret et al. 1995) to obtain a complete radio coverage for the drift bursts of interest in this study.

In the present paper we will check microwave images for flare wave signatures, with the aim of tracing the type II burst driver in low atmosphere and studying the shock association of type III bursts. This investigation requires high-cadence radio imaging in the low atmosphere, for which the Nobeyama Heliograph (NoRH) 17 GHz data are suitable. Therefore we make use of the 3 hr overlap between Potsdam and Nobeyama observing times. The NoRH (Nakajima et al. 1994) routinely images the Sun at 17 and 34 GHz in Stokes I and V, with spatial resolution of 10″ and 5″, respectively, and 1 s time resolution. The quiet-Sun emission at these frequencies has a brightness temperature of 10,000 K. Thermal bursts achieve 10^5 K and yield information about chromospheric and coronal plasma structures.

The data sources involved in our study cover a wide range of heights—from the chromosphere (some 1000 km above the photosphere) up to the transition in the solar wind. The lowest observing frequency (1 MHz) is emitted at about 8 $R_\odot$. Concerning the height coverage, there remains a gap between roughly 1.5 and 2.5 $R_\odot$ (40–14 MHz) in our data set. We use the metric–decimetric spectra to identify the type II burst, the microwave images to search for traces of the propagating disturbance, and the decametric–hectometric (Dm–Hm) spectra to detect low-frequency type III and type II bursts. Supplementary imaging information about the lower corona is gained from *SOHO*/EIT images, as well as from *Yohkoh*/SXT images. The present paper gives first results of this project.

2. OBSERVATIONS

In comparing the data archives from 1997 June till 1998 October of the Nobeyama 17 GHz radio heliograph with the AI Potsdam metric radio spectra, we found two events well suited for our study. Table 1 gives an overview of the parameters and data sources of these events.

2.1. *Meter-Wave Radio Spectral Data*

Figure 1 shows the radio dynamic spectra of both events, with high frequencies toward the top. At first glance, there are two basic differences between the events.

In event 1 (E1; Fig. 1*a*), type II bursts appear in a simple fundamental/harmonic mode (F/H) at 05:35–05:42 UT and between 100 and 40 MHz (*box II* in Fig. 1*a*). Earlier and at higher frequencies, type II precursor emission is detected (*box P* in Fig. 1*a*; see Klassen et al. 1999 for details). From the type II burst frequency drift, a speed of 610 km s^{-1} was estimated, applying the Newkirk (1961) density model. Between 05:25 and 05:32 and after 05:42, there are metric type III bursts up to the *Wind* frequency range. The type II signature disappears between 40 and 25 MHz (confirmed by Hiraiso 25–1000 MHz spectral observations). After 05:45 the type III bursts continuously change toward radio pulsations, with less and less Dm–Hm counterpart.

On the other hand, the type II burst in E2 (Fig. 1*b*) consists of two distinct bursts of different drift rate between 170 and 40 MHz and at 05:32–05:48 UT, both appearing in fundamental and harmonic mode. With the same density model as for E1, we obtain for the first burst (05:32:48–05:36:00 UT) a speed between 1250 and 1650 km s^{-1}. For the second burst (05:36:00–05:48 UT), we obtain a speed of 700–840 km s^{-1}. Note that 05:36 UT is when there occurs the transition between two different type II bursts and the onset of SA fast-drift bursts in E2. This plays an essential part in the further discussion.

In contrast with E1, E2 has almost no Dm–Hm type III bursts visible in the *Wind* spectrum in the time interval before and after the metric shock. But the coronal type II burst itself is accompanied by many type III bursts. It rather seems that the type III bursts emanate from the type II burst lane. The type III bursts are SA events (Cane et al. 1981; more recently discussed by Dulk et al. 2000). The first (faster) type II burst is continuously visible in the fundamental mode up to the 14–1 MHz range and disappears at about 4 MHz. Using the Mann et al. (1999) density model and the drift rate in the low-frequency range, we determine a velocity of 1390 km s^{-1}.

2.2. *Imaging E1: First a Moving Radio Source, Later an EIT Wave?*

In Figure 2 we present two difference frames of EIT 195 Å and NoRH 17 GHz radio images (05:37 subtracted from 05:24 UT).The EIT difference frame (Fig. 2*a*) shows a faint relative enhancement, which extends in projection on the disk toward the southeast. An arrow points to the leading part of the enhancement. Klassen et al. (2000) gave a speed of 260–320 km s^{-1} for this wave front segment. In the corresponding NoRH difference frame, two arrows are drawn to show the 17 GHz main stationary source within the active region and the moving source. The moving source almost coincides with the bright EIT enhancement, which is formed from the active region toward the southeast (see Fig. 2*a*). The time evolution of both radio sources and contrast-

TABLE 1

EVENT PARAMETERS AND INSTRUMENT INFORMATION

Parameter	Event 1 (E1)	Event 2 (E2)	Reference
Date	1997 Apr 2	1998 Jul 31	NOAA SGD[a] 638II (E1) and 653II (E2)
Time:			
Start (UT)	05:29	05:25	
Maximum (UT)	05:30	05:38	
End (UT)	05:65	06:15	
NOAA AR	8026	8283	
Position	S25 E05	N28 E31	
Hα imp.	SF	2F	
X-ray imp.	C 1.3	C 2.9	
Radio data:[b]			
1–14 MHz *Wind*	Yes	Yes	Bougeret et al. 1995
40–800 MHz AIP	Yes	Yes	Mann et al. 1992
800–2000 MHz AOO		Yes	Jiřička et al. 1993
17 GHz NoRH	Yes	Yes	Nakajima et al. 1994
X-ray data:			
Yohkoh SXT	Before 05:31 and after 07:50 UT	No	Tsuneta et al. 1991
Yohkoh HXT	No event	No	
BATSE	No event reported	No event reported	SDAC/GSFC[c]
SOHO[d] data:			
EIT 195 Å	05:24; 05:36	Mission interrupted	Fleck, Domingo, & Poland 1995
LASCO C2 CME	07:17 UT; P.A. 72°; 338 km s^{-1}	No CME observation	St. Cyr 1999, private communication

[a] NOAA SGD: National Oceanic and Atmospheric Administration, Solar Geophysical Data.
[b] AIP: AI Potsdam; AOO: Astronomical Observatory Ondřejov.
[c] SDAC/GSFC: Solar Data Analysis Group at Goddard Space Flight Center.
[d] *SOHO*: *Solar and Heliospheric Observatory*; EIT: Extreme-Ultraviolet Imaging Telescope; CME: coronal mass ejection.

enhanced enlargements of the moving source are offered in Figure 3. Figure 3*b* shows that the radio source moves toward the southeast at the projected speed of 370 ± 130 km s^{-1}. Figure 3*a* shows that the moving blob and the stationary main source emit thermal radiation at (10–25) × 10^3 K. We note that in *SOHO*/LASCO C2 coronagraph images an event was noted starting at 07:17 UT at PA 72° (see Table 1). It has a constant speed of 338 km s^{-1} and was characterized as "faint material, followed by something bright" (C. St. Cyr, CME list 1997 on the *SOHO*/LASCO Web site).[1]

2.3. *Imaging E2: A Moving Disturbance Hits a Remote Prominence*

In Figures 4 and 5, we present the 17 GHz imaging information. Figure 4*a* shows a full-disk image during the flare onset in NOAA Active Region (AR) 8283. The three regions marked A, D, and F are important for the following discussion. A is the site of the flare onset at 17 GHz and in soft X-rays at 05:28 UT. D is a region of rectangular shape that lies to the east of the active region and shows a transient decay of emission between 05:31 and 05:33. Region D is denoted by a white arrow in the enlargement in Figure 4*b*. Finally, F is the almost north-south extended quiescent filament that plays an important part in the further evolution of the flare signatures initiated in NOAA AR 8283.

The magnetic configuration leading to the preflare rectangular 17 GHz source arrangement is due to a concentration of south-field polarity encircled by distributed north-field polarity (A. Hofmann 1999, private communication). The 17 GHz sources are situated in the footpoints of loops, with about 5000 km turning height. The flare is situated in the western part of the rectangular pattern (at site A). In the preflare stage the rectangular 17 GHz source pattern is almost closed. Later, between 5:31 and 5:33 UT, an eastward-escaping, well-focused disturbance darkens a part of the eastern branch of the source arrangement (site D). In the north of the flare site A, a pair of 17 GHz sources separates from each other. We have inserted crosses and black arrows in Figure 4*b* to clearly show this motion. We argue that these are footpoint sources in a narrow and extended loop. The footpoint expansion speed is 135–220 km s^{-1}. There are no Hα data available for this event, so we cannot compare this speed with any flare ribbon expansion. Anyway, we would not expect nicely expanding flare ribbons, because E2 is more a confined event.

The evolution of the flare-ejected 17 GHz absorbing cloud after it passes region D is presented in Figure 5. From 5:33 to 5:42 UT, the flare-ejected absorbing matter moves across the disk toward the east, thereby screening the background 17 GHz emission. We demonstrate this with three selected frames (Fig. 5*a*) and by one-dimensional scans of brightness temperature from the east limb to the region west of D (Fig. 5*b*). For the absorption maximum (*crosses*) we have determined a projected eastward speed of 216 ± 10 km s^{-1}. Eventually, the disturbance hits the remote quiescent prominence F. The collision is best visible in the 05:36–5:38 UT images. The simultaneous formation of electron beams is evidenced by the shock-associated (SA) Dm–Hm type III bursts at 05:36 UT (Fig. 1*b*). We have enlarged the most interesting time and frequency interval of the spectrum in Figure 7. Fundamental and harmonic mode signatures of the first type II burst are marked. Between these features many superposed fast-drift bursts can be recognized (labeled SA). Among them (between 40 and 50 MHz) there are also positively drifting strong herringbones.

[1] Available at http://lasco-www.nrl.navy.mil/cmelist.html.

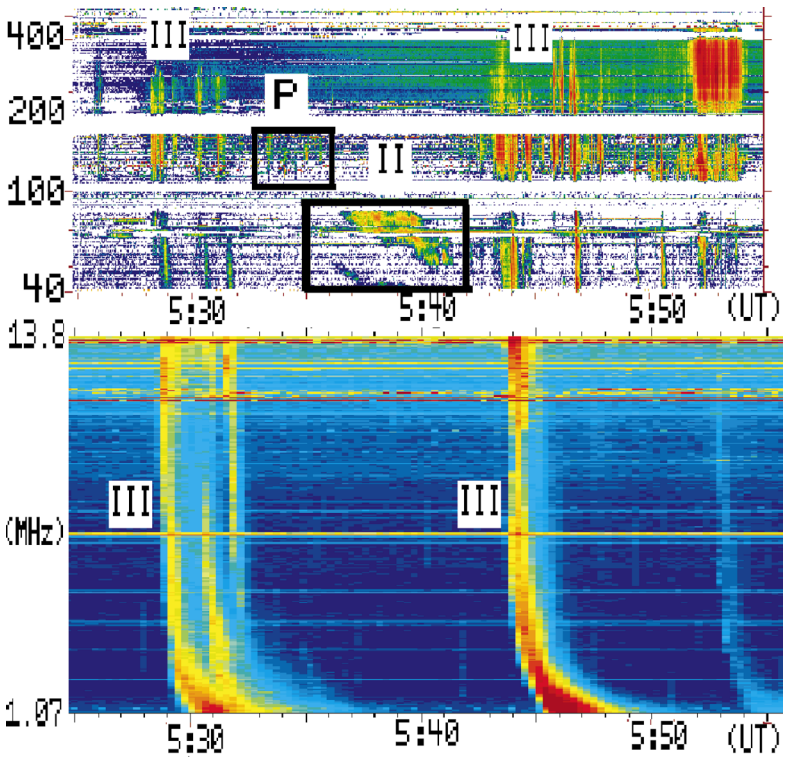

FIG. 1*a*

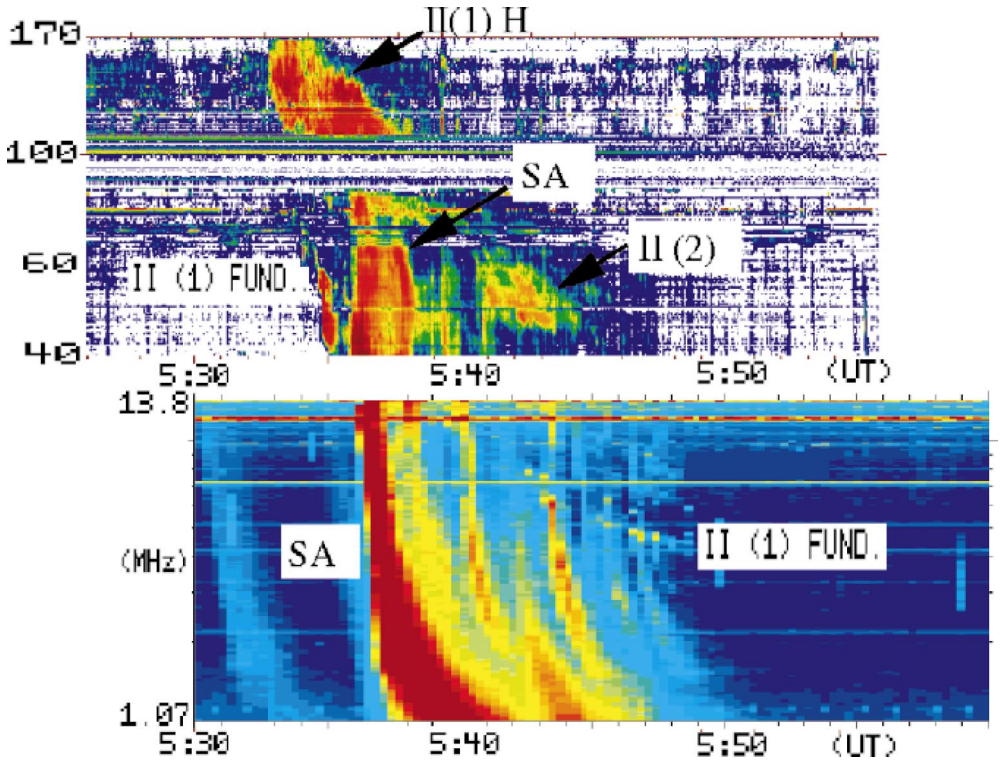

FIG. 1*b*

FIG. 1.—Radio spectra for (*a*) 1997 April 2 (E1) and (*b*) 1998 July 31 (E2); frequency-time plane according to the convention of the low-frequency radio astronomy. The spectra of 400–40 MHz in *a* and 170–40 MHz in *b* are from AI Potsdam; 13.08–1.07 MHz data are from *Wind*. In E1 a metric type II burst appears *between* groups of metric/hectometric type III bursts. On the contrary, in E2 the metric type II burst occurs *together* with hectometric type III bursts. In *a*, P marks the precursor and II the type II burst. In *b*, there are two coronal type II bursts in the interval 05:32–05:49 UT. The first type II burst [F-mode, II(1) FUND], appears almost continuously in 70–4 MHz. II(2) H (H-mode) marks the second type II burst and SA the shock associated event.

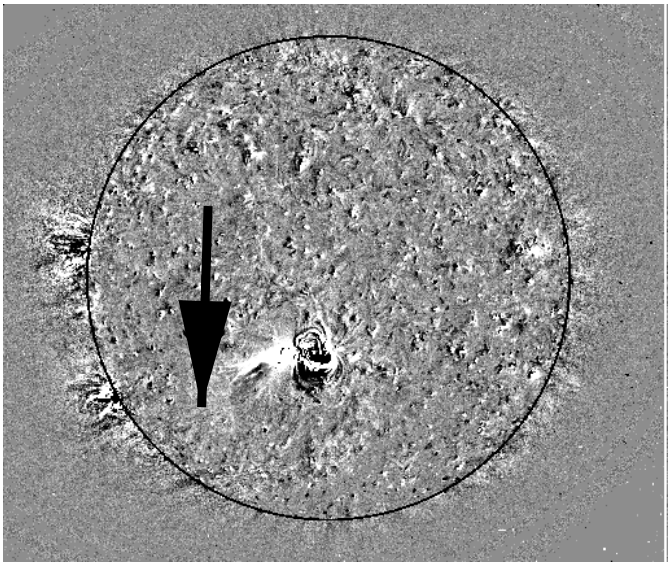

FIG. 2*a*

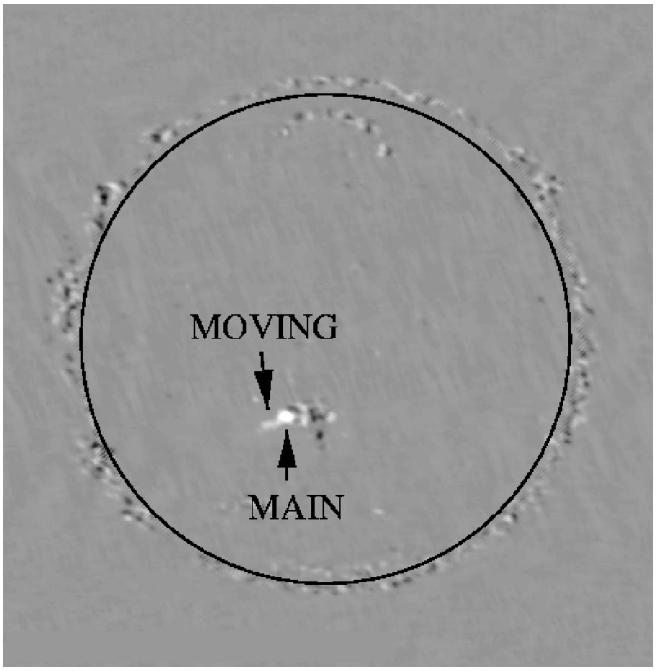

FIG. 2*b*

FIG. 2.—The 1997 April 2 event (E1). Difference frames (05:37 minus 05:24 UT) from (*a*) *SOHO*/EIT 195 Å and (*b*) NoRH 17 GHz images. EIT images are from Klassen et al. (2000). In *a*, white represents enhanced emission and black the relative dimming. The arrow in *a* points at an eastward-moving faint enhancement (EIT wave front segment). Arrows in *b* indicate the stationary main and the moving secondary sources. See also Fig. 3.

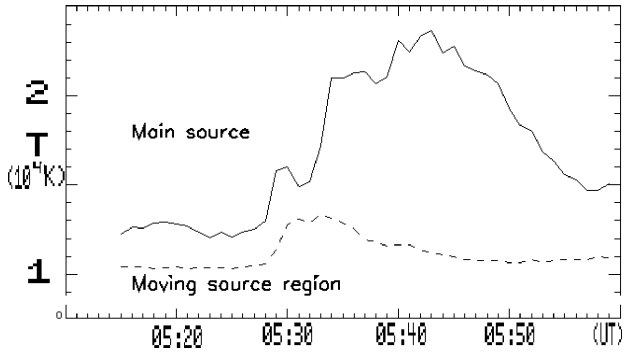

FIG. 3*a*

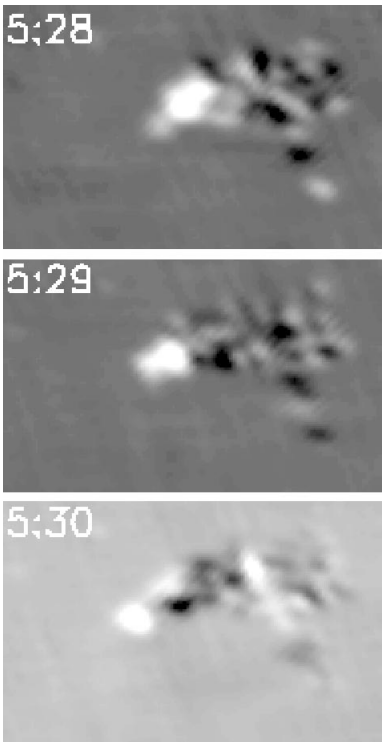

FIG. 3*b*

FIG. 3.—Details of the 1997 April 2 event (E1) at 17 GHz (compare with Fig. 2). (*a*) The brightness temperature evolution of the 17 GHz main and moving sources. (*b*) Time sequence (05:28–05:30 UT) of the enlarged part of the flaring active region. A mean preflare image was subtracted, and each image shows the difference with the previous one (i.e., 5:28 means 5:28 minus 5:27 UT, etc.). Thus, in *b* the (stationary) main source is almost invisible, while the moving source can be clearly recognized.

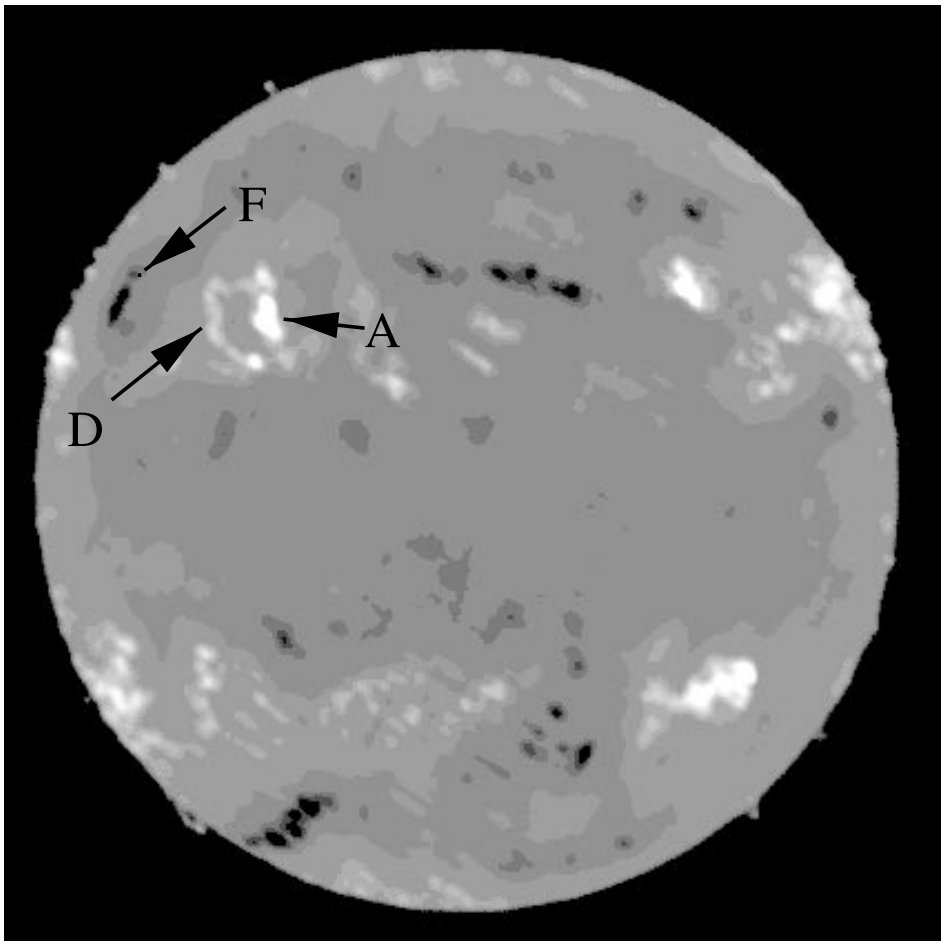

FIG. 4*a*

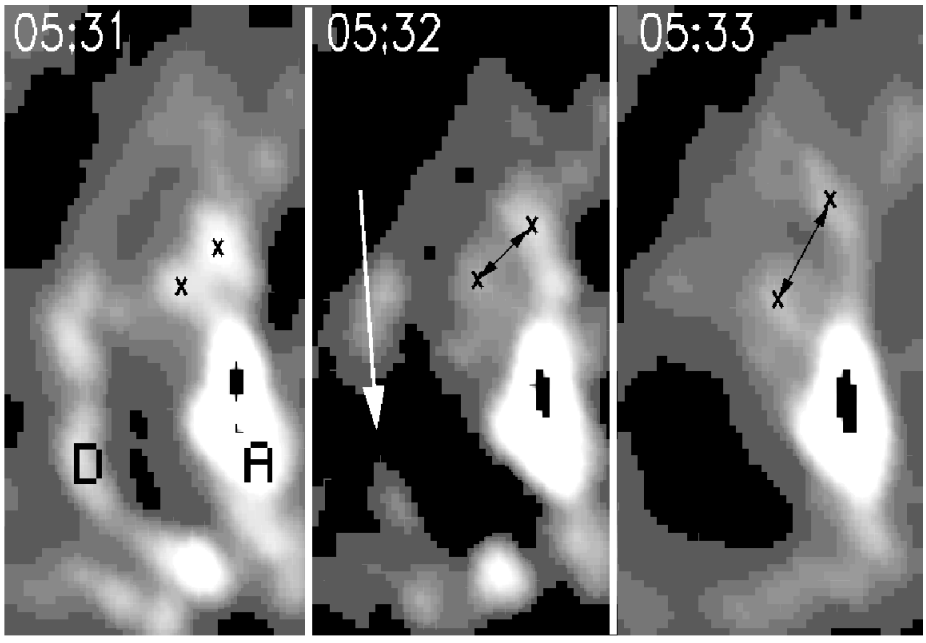

FIG. 4*b*

FIG. 4.—Selected NoRH 17 GHz images of the 1998 July 31 event (E2). (*a*) Full-disk (05:30 UT): flare onset at 05:28 UT (A), temperature depression at 05:32 UT (D), and north-south extended quiescent prominence (F). (*b*) Closer look at the A–D region at 05:30–05:32 UT. Black pixels within the very bright regions are due to saturation. The release of the absorbing cloud toward the east (*white arrow*; microwave dimming) is visible. In the north of region A, an expanding double source is marked by black crosses and arrows.

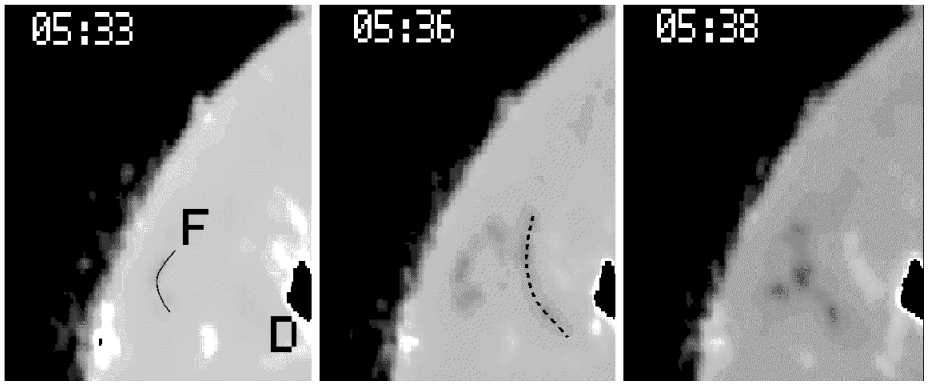

FIG. 5*a*

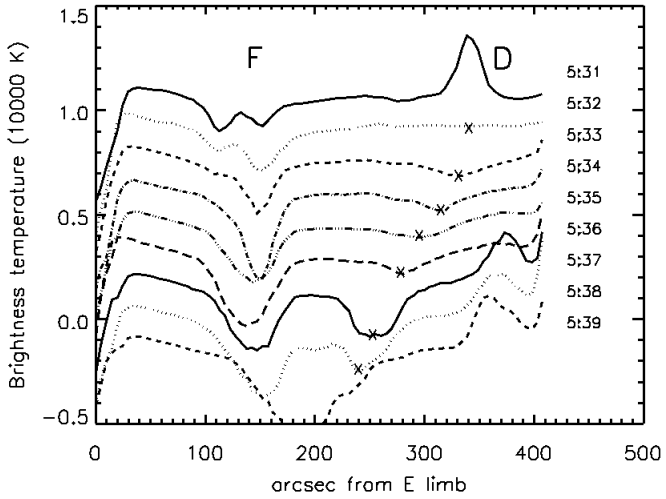

FIG. 5*b*

FIG. 5.—The 1998 July 31 event (E2), 17 GHz NoRH data. (*a*) Selected images showing the propagating absorption cloud and the prominence (F in Fig. 4). (*b*) One-dimensional scan of the brightness temperature from east to west between the east limb and regions F and D. Times are shown in UT. Curves are shifted by −1500 K per minute. The propagating temperature minimum is denoted by X.

The flare-related disturbance, when it reaches the limb at the north of region F, looks like a narrow loop prominence rising between 5:45 and 5:50 UT. We obtained a velocity estimate of 310 km s^{-1}. Simultaneously with its disappearance, the Dm–Hm type II and SA type III signatures cease.

2.4. *Decimeter Bursts during Metric Type II Bursts and the 17 GHz Absorbing Cloud*

As discussed in § 2.1, two type II bursts are observed in sequence during E2. The 40–800 MHz spectrum of the first (Fig. 1*b*) is shown enlarged in Figure 6*a*. The fundamental mode component of this burst brightens at 75 MHz about 1 minute after the harmonic mode start at 05:33–05:34 UT and at about 150 MHz. This is when the absorption minimum (X) leaves position D (see Fig. 5*b*, curves 05:33 and 5:34 vs. 05:31 UT). The spectrum reveals more about faint bursts around 300 MHz and later between 400 and 200 MHz. No bursts are detected between 800 and 400 MHz. At 05:36 UT the SA burst onset is well visible (Fig. 7). In Figure 6*b*, we give a 1–2 GHz spectrum of a number of decimetric reverse-drift bursts appearing mainly in the time interval of enhanced fundamental mode type II burst flux. Note the decay tendency of the start frequency of the reverse-drift bursts. The frequency drift of the single bursts is low (about +250 MHz s^{-1}) for reverse-drift bursts in this frequency range.

The decimeter bursts show some similarity with herringbone emission (Nelson & Melrose 1985) during meter-wave type II bursts. They become visible just together with the fundamental mode meter-wave type II burst, during the time interval of undisturbed propagation of the 17 GHz absorbing cloud from D to F (see Fig. 5). We consider that this may indicate the change of radio wave escape conditions after the cloud leaves the loop structures of the flaring active region.

3. DISCUSSION

The present observations revealed that the moving 17 GHz source coincides with the EIT wave formation in E1 and with remote prominence destabilization in E2, in terms of time, speed, and direction. The EIT waves are well correlated with metric type II bursts (Klassen et al. 2000). The observed prominence destabilization occurs simultaneously with a drastic change in the spectrum of a preexisting type II burst and with the formation of shock-associated (SA) metric and decimetric radio features. These results suggest a causal connection between the observed moving microwave

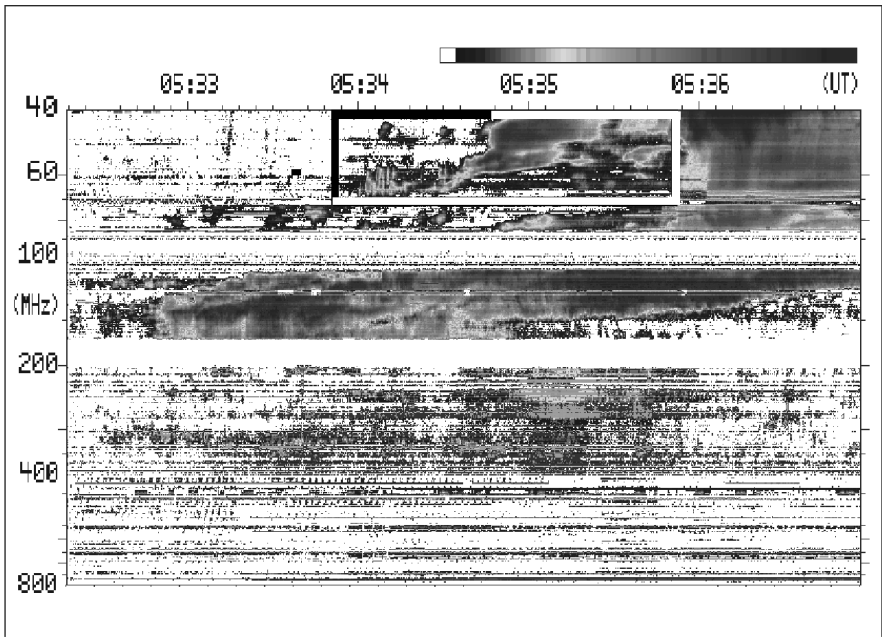

FIG. 6*a*

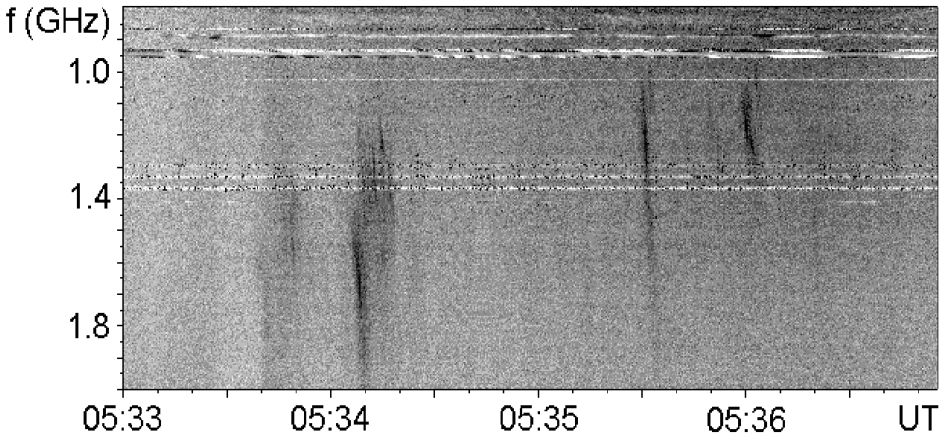

FIG. 6*b*

FIG. 6.—Radio spectra of the 1998 July 31 event (E2). (*a*) Metric type II burst components (AI Potsdam; logarithmic frequency scale). The box contains the fundamental mode features of the first type II burst. (*b*) Simultaneously observed decimeter reverse-drift bursts with decreasing start frequency (Astronomical Observatory Ondřejov; linear frequency scale). Note that the reverse-drift bursts appear mainly during the fundamental mode type II emission in *a*.

features and the disturbance that grows to a flare shock capable of exciting type II burst emission. We call this disturbance the type II burst driver; it might be a flare blast wave or a massive piston (see, e.g., Cliver et al. 1999; Vršnak & Lulič 2000a, 2000b).

Because we used different sets of partly spectrographic and partly imaging data to give a comprehensive picture of the processes, we organize our findings in a schematic form in Figure 8 for E1 and Figure 9 for E2.

3.1. *Microwave Signature of the Type II Burst Driver?*

We found in both flares a moving disturbance in 17 GHz radio images, occurring earlier than the type II radio burst in the meter-wave range. Both timing and propagation direction of the moving exciter are in favor of the idea that they trace the flare-induced shock-exciting disturbance. We identified a source of additional microwave emission (E1) and a source absorbing the chromospheric 17 GHz radio background (E2). Both disturbances move with a speed in the range of average coronal EIT wave velocities (Klassen et al. 2000) and are detected at 17 GHz but not at 34 GHz.

In the case of E1 (see the summary in Fig. 8), we observe the 17 GHz source moving with a projected speed of about 370 ± 130 km s^{-1}. Immediately thereafter, a stationary 17 GHz source (called the main source) is formed at the starting point of the moving source. The moving 17 GHz source occurs together with a group of metric type III bursts. The corresponding beams escape into the heliosphere and induce decametric and hectometric type III emission. Metric type II burst precursor emission (Klassen et al. 1999; *region P* in Fig. 1*a*) follows in the dynamic radio spectrum. Linearly extrapolating the motion of the microwave source into the disk leads to a bright arc—an EIT wave front segment—in the EIT image difference frame 05:37 minus

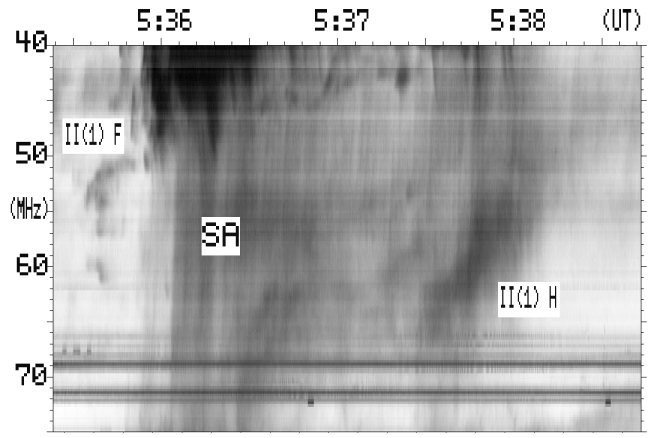

FIG. 7.—Radio spectrum of the 1998 July 31 event (E2) during the impact of the shock wave on the quiescent prominence and SA burst formation. The 05:36 UT 17 GHz brightness scan (Fig. 5*b*) is still undisturbed concerning the prominence and the absorbing cloud positions. II(1) F and II(1) H mark the first type II burst fundamental and harmonic modes, respectively; SA marks the shock-associated type III bursts. In this figure, no background subtraction was carried out.

05:24 UT (Fig. 2*a*). Assuming wave starting times between 5:26 and 5:28 UT (the first X-ray effect and the first microwave flare source occurrence, respectively), one obtains wave speeds between 260 and 320 km s^{-1}. The speed of the EIT wave front segment agrees with that of the moving microwave source within the uncertainties of the measurements. It is likely that we may have observed a microwave source that is causally related to the later-visible EIT wave. Later, faint CME appears in the LASCO coronagraph field of view at a constant speed of 338 km s^{-1}, which is in good agreement with the speed values determined from the 17 GHz microwave images. In the perspective of E1, one might be inclined to assume (following Delannée, Delaboudinière, & Lamy 2000) that we have seen the formation of a flare-related, looplike faint mass ejection, dominantly the projection of its eastern rim onto the disk. Despite coinciding projected speeds, the motion between EIT and LASCO C2 images was not continuous. The CME occurs too late (see Table 1).

In the case of E2 (see the summary in Fig. 9), we are faced with a different indication of a moving disturbance. Starting from the energy release site, a moving cloud of cold and dense (17 GHz absorbing) plasma is detected in front of the quiet-Sun chromosphere. This motion is eastward across the disk, with a constant projected speed of 216 ± 10 km s^{-1}. The absorbing matter is initially visible during its crossing of the eastern part of the rectangular 17 GHz preflare pattern (Fig. 4*b*). Before 05:29–05:30 UT (not shown here), we see the first type II–related signature. It is a lane of precursor emission, including type U bursts (Klassen et al. 1999), with the same envelope drift rate as later found for the first type II burst lane.

The proper type II burst starts with strong harmonic mode emission during the screening of the eastern part of the rectangular 17 GHz source pattern. As soon as the cold plasma cloud has passed over region D, the type II burst spectrum changes so that the fundamental mode becomes clearly visible (Fig. 6*a*, *box*). In the same time interval, we see a possibly type II–like decimetric feature (Fig. 6*b*) between 1 and 2 GHz. The appearance of the fundamental mode type II emission, as well as the simultaneous appearance of decimetric bursts, points to a change of radio wave escape conditions.

After four minutes of undisturbed propagation (see Figs. 5*b* and 9, 05:32–05:36 UT), the absorbing cloud interacts with a preexisting quiescent prominence. In the same time interval, the metric type II burst drastically changes its appearance. Strong fast-drift burst features appear (Fig. 7). Simultaneously, shock-associated Dm–Hm type III bursts are seen in the *Wind* data (see Fig. 1*b*). After the interaction of the disturbance with the prominence, a slower drifting type II burst lane is seen between 40 and 70 MHz. The estimated shock speed is about half the speed derived for the first type II burst. In the same time interval, the fundamental mode emission of the first type II burst extends down to about 4 MHz. We conclude that a part of the shock front escapes more or less radially without interacting with the prominence.

The details of the prominence-cloud interaction revealed by the 17 GHz images are interesting (see Fig. 9*a*). Initially, the east-west brightness distribution shown in Figure 5*b* depicts the expected pattern: the cloud moves toward the undisturbed prominence. The last profile with this information is that from 05:36 UT. At 05:37 UT, the prominence moves slightly toward the approaching cloud of absorbing matter. At 05:38 UT, both absorption effects are melting together in the midst of the remaining path between the prominence and the cloud. This may be understood as follows: the absorbing cloud probably moves with the downstream plasma speed behind the super-Alfvénic shock wave. Therefore, the shock wave in front of the cloud arrives earlier (and probably also at a greater height) than the absorbing cloud. This leads to the (at first glance surprising) fact that the prominence body is strongly disturbed before the arrival of the absorbing cloud.

To summarize, in both cases we can detect, immediately before and during the metric type II burst, the slowly moving 17 GHz features. Assuming coronal propagation and a coronal sound speed of about 190 km s^{-1} (Klassen et al. 2000), we note that the speed of the tracer is supersonic even in projection. The disturbance moves with high directivity, partly because of its excitation and partly because of the conditions in the surrounding corona. The speed is significantly lower than those estimated from type II burst drift rates, even if using density models for an open magnetic field (see, e.g., Newkirk 1961; Mann et al. 1999).But it is well within the range of the EIT wave speed, as found statistically (Klassen et al. 2000) and by modeling the surface-projected propagation of an initially sub-Alfvénic fast mode disturbance (Wang 2000).

3.2. *SA Events: Shock-associated or Shock-accelerated?*

One of the substantial differences between the two events is the association between metric type II burst lanes and low-frequency, interplanetary type III bursts (Fig. 1).

In the case of E1, it is not clear if the missing type III bursts during the metric type II burst (see the low-frequency radio spectrum during the time interval of box II in Fig. 1*a*) are causally related with the associated coronal disturbance. East of NOAA AR 8026, new magnetic flux appears on 1997 April 2; it reforms the magnetic structure of this region and probably causes, among others, the observed flare (A. Hofmann 1999, private communication). We mentioned

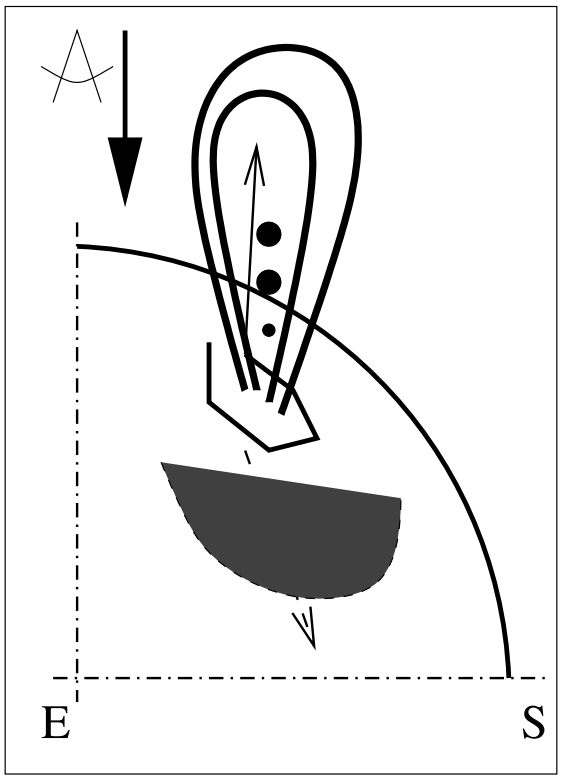

FIG. 8*a*

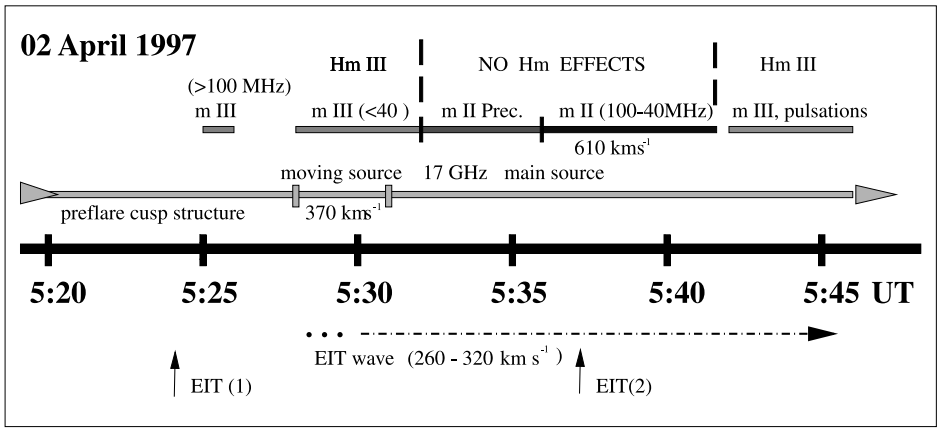

FIG. 8*b*

FIG. 8.—The 1997 April 2 event (E1): (*a*) schematic plot; (*b*) time line scheme demonstrating how the different observations fit together. "Prec." means precursor (Klassen et al. 1999). Compare this scheme with Figs. 2 and 3. In *a*, the circles and arrow symbolize the moving 17 GHz source. It is surrounded by an expanding, eastward-inclined coronal structure drawn here as a loop. Possibly, in this case, the projection of this structure on the disk yields the EIT wave front segment (*shaded region in a, dot-dashed line in b*).

above that the type III emission drastically changes its total bandwidth during the flare. In the beginning it spans 2.5 decades in frequency (see the time interval 05:28–05:32 UT in Fig. 1*a*). At the end it is almost reduced to broadband pulsations in the range 400–200 MHz (past 05:50 UT in Fig. 1*a*).

As we have seen in E2, the type III emission is excited during the collision between the shock wave (which probably leads the absorbing cold matter; see features II and X in Fig. 9) and the quiescent prominence (feature F in the same figure). This process drastically changes the spectrum of the type II burst (see Figs. 1*b*, 6*a*, and 7). On the other hand, it leads to the emission of the bunch of type III bursts (SA in Fig. 1*b*). We see alternative possibilities for understanding the sudden formation of electron beams in the given situation:

1. On top of the prominence a streamer structure is expected, as sketched in Figure 9*a*. Because of the shock wave impact, the prominence-streamer system gets disturbed. Small-scale energy release by reconnection can lead to electron beam acceleration. In comparison, Klein et al. (1997) have observed this process as a spontaneous one (without the action of a shock wave) within 5 hr before a

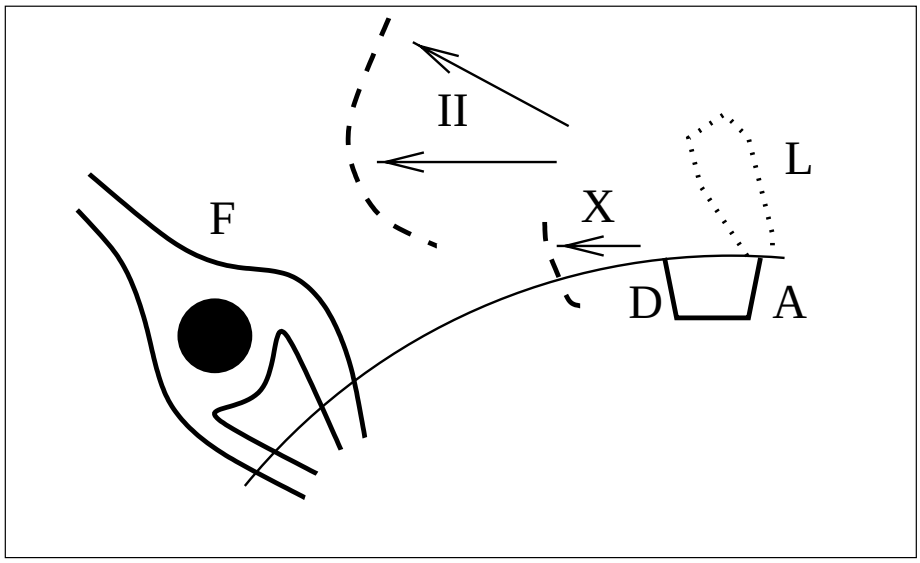

FIG. 9*a*

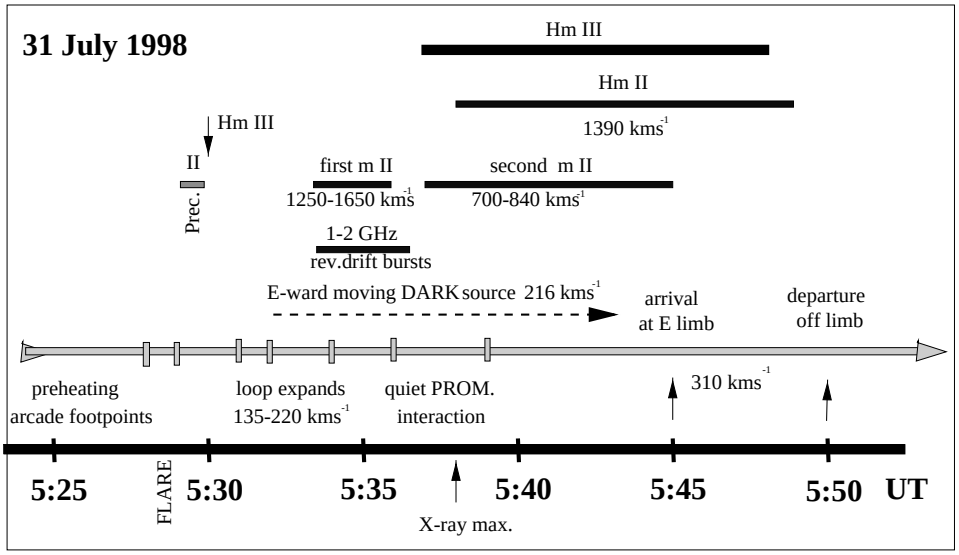

FIG. 9*b*

FIG. 9.—Same as Fig. 8, but for the 1998 July 31 event (E2). In *a*, A, D, and F are the regions so marked in Figs. 4 and 5, X is the propagating brightness minimum, II is the metric type II burst source, and L is the expanding loop seen in the active region (see Fig. 4*b*) and, later, over the east limb.

prominence eruption. Odstrčil & Karlický (1997) have shown how a shock wave triggers reconnection in a streamer's current sheet.

2. If the shock carries an ensemble of accelerated electrons (see, e.g., Vandas & Karlický 2000), these can be released from the shock frame because of the interaction between the shock wave and the streamer structure. Because of the impact there is no acceleration, but only a release of preaccelerated electrons.

3. During the collision between the shock wave and the prominence-supporting magnetic system, there arises a magnetoplasma structure that is extremely suitable for accelerating electrons (e.g., approaching magnetic mirrors; Mann 1995).

In case 1, the electron beams are not accelerated, but their release is stimulated by the arriving shock wave. In cases 2 and 3, the collision between the wave and a preexisting plasma–magnetic field configuration is essential to release the beams. In any case, the streamer field lines allow the electrons to escape toward the heliosphere. Aurass, Hofmann, & Urbarz (1998) described a similar case, seen in meter-wave imaging data, where a type II burst changes its lane structure and releases streams of type III emitting electrons as a result of its interaction with a unipolar magnetic structure above a weak field area well away from the flaring active region.

From the observational point of view, discrimination among these is impossible in the given situation. In contrast with Dulk et al. (2000), we stress that the simultaneous appearance of type II and type III bursts in spectral data does not necessarily mean that the type III bursts are due to shock-accelerated electrons. We have no doubt that coronal shock waves can accelerate electrons, as we see in the type II bursts. But our results show that the sources of electron streams in the heliosphere may not be magnetically rooted

just in a flaring active region, even if the electron streams are well flare-associated in time. So, some discrepancy in backtracing heliospheric effects to the Sun and to the actual solar active region may be understood.

4. CONCLUSIONS

In the present paper, analysis of high time resolution radio data in the range between 17 GHz and 1 MHz is made for two comparatively simple flare events. We focus on the problems of (1) detection of the possible driver of the type II burst and (2) conditions for SA event formation.

For both flares we found traces of the type II burst–exciting disturbances in high-frequency radio emission: in E1 a dense moving source emitting thermal radiation at 17 GHz and in E2 an absorption feature on the background of chromospheric radio emission. Both tracers move at a projected supersonic speed between 200 and 400 km s^{-1}, which lies well within the velocity range of the EIT waves. Moreover, we have shown that an EIT wave front may plausibly correspond to the motion of a (meanwhile extinguished) moving microwave source.

Further, we have demonstrated that the spectral appearance, as well as the drift rate, of a type II burst can change when the flare-related disturbance encounters a massive obstacle—a quiescent prominence—comparatively far out of the flaring active region. During this impact, typical SA type III bursts are excited. We cannot determine if the type III electron beams are only shock-associated or really shock-accelerated. Although we cannot prove it with the metric imaging data, our results make it probable that SA type III burst radio sources can appear well away from the flare site, on field lines connected with the interaction region between the flare disturbance and the obstacle.

Finally, we found (for E2) some evidence that the same disturbance leading to the excitation of a metric type II burst can induce herringbone-like decimetric radio signature, despite a spectral gap between the type II and the decimeter reverse-drifting bursts.

H. A. is grateful to the Japan Society for the Promotion of Science and to the Deutscher Akademischer Austauschdienst for supporting his stays at Nobeyama National Radio Astronomy Observatory and at ISAS Sagamihara. Further, he acknowledges the advice of J. Khan, H. Hudson, and his Japanese colleagues in analyzing *Yohkoh* data. His thanks are due to B. Thompson, A. Hofmann, C. St. Cyr, B. Vršnak, and to his colleagues from AIP Solar Radio Group for useful discussions. This work was significantly improved by the comments of an unknown referee.

REFERENCES

Aurass, H., Hofmann, A., & Urbarz, H.-W. 1998, A&A, 334, 289
Bougeret, J.-L., et al. 1995, Space Sci. Rev., 71, 231
Cane, H. V., Stone, R. G., Fainberg, J., Steinberg, J. L., Hoang, S., & Stewart, R. T. 1981, Geophys. Res. Lett., 8, 1285
Cliver, E. W., Webb, D., & Howard, R. A. 1999, Sol. Phys., 187, 89
Delannée, C., Delaboudinière, J.-P., & Lamy, P. 2000, A&A, 355, 725
Dulk, G. A., Leblanc, Y., Bastian, T. S., & Bougeret, J.-L. 2000, J. Geophys. Res., 105, 27343
Fleck, B., Domingo, V., & Poland, A. I., eds. 1995, The *SOHO* Mission (Dordrecht: Kluwer)
Hudson, H. S., & Karlický, M. 2000, in ASP Conf. Ser. 206, High Energy Solar Physics: Anticipating HESSI, ed. R. Ramaty & N. Mandzhavidze (San Francisco: ASP), 268
Jiřička K., Karlický M., Kepka O., & Tlamicha, A. 1993, Sol. Phys., 147, 203
Khan, J. I., & Aurass, H. 2001, A&A, in press
Klassen, A., Aurass, H., Klein, K.-L., Hofmann, A., & Mann, G. 1999, A&A, 343, 287
Klassen, A., Aurass, H., Mann, G., & Thompson, B. J. 2000, A&AS, 141, 357
Klein, K.-L., Aurass, H., Soru-Escaut, I., & Kálmán, B. 1997, A&A, 320, 612 (erratum 322, 1027)
Klein, K.-L., Khan, J. I., Vilmer, N., Delouis, J.-M., & Aurass, H. 1999, A&A, 346, L53
Mann, G. 1995, in Lecture Notes in Physics 444, Coronal Magnetic Energy Release, ed. A. O. Benz & A. Krüger (Berlin: Springer), 183
Mann, G., Aurass, H., Voigt, W., & Paschke, J. 1992, in Coronal Streamers, Coronal Loops, and Coronal and Solar Wind Composition: The First *SOHO* Workshop, ed. C. Mattok (ESA SP-348; Noordwijk: ESA), 129
Mann, G., Classen, T., & Aurass, H. 1995, A&A, 295, 775
Mann, G., Jansen, F., MacDowall, R. J., Kaiser, M. L., & Stone, R. G. 1999, A&A, 348, 614
Moreton, G. E., & Ramsey, H. E. 1960, PASP, 72, 357
Nakajima, H., et al. 1994, Proc. IEEE, 82, 705
Nelson, G. J., & Melrose, D. B. 1985, in Solar Radiophysics, ed. D. J. McLean & N. R. Labrum (Cambridge: Cambridge Univ. Press), 333
Newkirk, G., Jr. 1961, ApJ, 133, 983
Odstrčil, D., & Karlický, M. 1997, A&A, 326, 1252
Pohjolainen, S., et al. 2001, ApJ, 556, 421
Suzuki, S., & Dulk, G. A. 1985, in Solar Radiophysics, ed. D. J. McLean & N. R. Labrum (Cambridge: Cambridge Univ. Press), 289
Thompson, B. J., Plunkett, S. P., Gurman, J. B., Newmark, J. S., St. Cyr, O. C., & Michels, D. J. 1998, Geophys. Res. Lett., 25, 2465
Thompson, B. J., Reynolds, B., Aurass, H., Gopalswamy, N., Gurman, J. B., Hudson, H. S., Martin, S. F., & St. Cyr, O. C. 2000, Sol. Phys., 193, 161
Tsuneta, S., et al. 1991, Sol. Phys., 136, 37
Vandas, M., & Karlický, M. 2000, Sol. Phys., 197, 85
Vršnak, B., & Lulič, S. 2000a, Sol. Phys., 196, 157
———. 2000b, Sol. Phys., 196, 181
Wang, Y.-M. 2000, ApJ, 543, L89
Warmuth, A., Hanslmeier, A., Messerotti, M., Cacciani, A., Moretti, P. F., & Otruba, W. 2000, Sol. Phys., 194, 103
Warmuth, A., Vršnak, B., Aurass, H., & Hanslmeier, A. 2001, ApJ, 560, L105